Nuclear Materials and Energy 32 (2022) 101203

Contents lists available at ScienceDirect

Nuclear Materials and Energy

journal homepage: www.elsevier.com/locate/nme

Stress distribution in a 316L(N) steel narrow gap TIG model weld for Gen IV nuclear applications

P. Agostini [a], R. Coppola [b,*], M. Hofmann [c], C. Ohms [d], K. Tucek [d]

[a] ENEA-Brasimone, FSN-ING, CP 1, 40032 Camugnano (BO), Italy
[b] ENEA-Casaccia, FSN-ING, Via Anguillarese 301, 00123 Roma, Italy
[c] Heinz Maier-Leibnitz Zentrum (MLZ), Technische Universität München, Lichtenbergstrasse 1, Garching 85748, Germany
[d] European Commission, Joint Research Centre, Westerduinweg 3, 1755 LE Petten, The Netherlands

ARTICLE INFO

Keywords:
Neutron diffraction
Stress measurements
Nuclear welds
Nuclear safety

ABSTRACT

The stress distribution in a model weld developed for nuclear application has been determined non-destructively by means of neutron diffraction, in the frame of the Horizon 2020 Project Generation IV Materials Maturity (GEMMA). The investigated sample is a narrow gap Tungsten Inert Gas (TIG) austenitic 316L(N) steel weld, prepared following RCC-MRx Code specifications. Two lines perpendicular to the welding direction, at the middle of the sample, were scanned at 6 mm and 14 mm depth; additional measurements were carried out in the middle of the weld, down to 16 mm depth. At 6 mm depth and within ± 5 mm distance from the weld centre, marked tensile stress gradients are found, with the residual stresses reaching maximum values up to 400 MPa in the longitudinal direction. At 14 mm depth, the stresses decrease to around 200 MPa for the longitudinal component and get compressive for the transverse and normal components, down to −200 MPa for the transverse one, with smoother stress gradients around the weld. The in-depth measurements inside the weld confirm that the main integrity concern for the investigated sample may arise from the tensile longitudinal stresses. Additional micro-structural information has been obtained by qualitative comparison of diffraction line profiles in the weld and in the base metal. These experimental results are discussed with reference to the expected service conditions of such welds and to their capability to fulfill Gen IV safety goals and requirements.

Introduction

Compared to present commercial light water reactors, next generation nuclear systems such as Gen IV reactors will require structural materials and related technologies capable to withstand more challenging operating conditions [1-3], namely: operation temperatures well above 350 °C, irradiation doses up to 200 dpa (displacement per atom), required compatibility with more corrosive coolants and an expected lifetime of 60 years [4,5]. The Gen IV systems also need to demonstrate robust safety and reliability under off-normal and accidental conditions. More specifically, the higher operation temperatures are harmful to steel welds, particularly in their Heat Affected Zones (HAZ) [6]. In order to prevent failure because of weld cracking, innovative welding protocols must be defined and theoretical predictions of weld performance must be experimentally validated. Therefore, the component design codes such as the RCC-MRx [7] also need to be reviewed and partially extended, based on scientific findings and operating experience feedback, in order to provide detailed guidance for ensuring that components fulfill the safety and technical requirements, while remaining cost-competitive.

In this context, reliable knowledge of residual stresses in components is fundamental, since in nuclear welds the residual stresses act as "secondary stresses"; they add to the primary thermal and mechanical operational cyclic loads and this combination can lead to localized permanent deformation in a component or to cracking. The cyclic thermal loading problem is further complicated by the structure of Gen IV systems, utilizing molten salt, sodium or lead as coolant; in fact, in proximity of the coolant free surface, alternating wet/dry conditions produce corresponding temperature and stress gradients, resulting in ratcheting or fatigue of the vessel itself. That is schematized in Fig. 1 [8], representing the progressive deformation of a cylinder cyclically subjected to a temperature gradient traveling in the axial direction, with no primary loads applied: during the operation, the coolant level moves up and down with corresponding variation in temperature distribution on

* Corresponding author.
E-mail address: roberto.coppola@enea.it (R. Coppola).

https://doi.org/10.1016/j.nme.2022.101203
Received 2 November 2021; Received in revised form 23 May 2022; Accepted 24 May 2022
Available online 26 May 2022

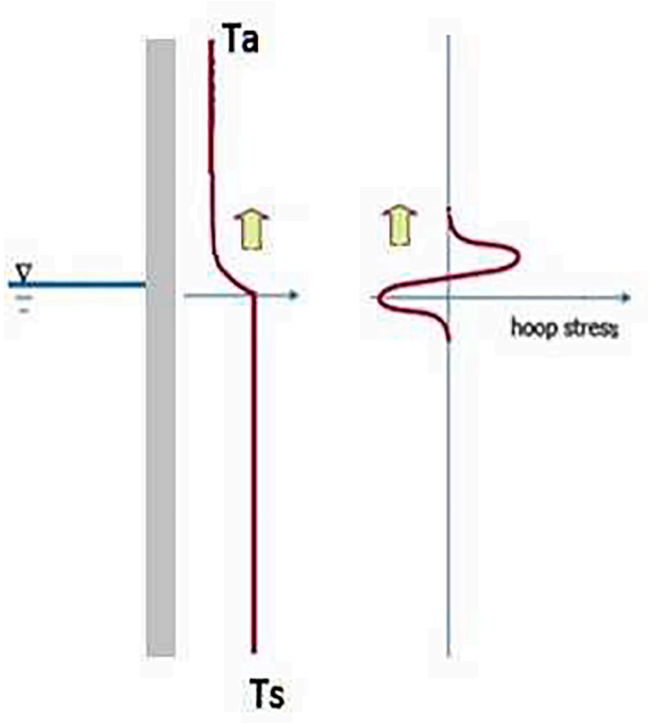

Fig. 1. Origin of the temperature controlled secondary stresses in a welded vessel, cooled by molten salt. The horizontal blue line indicates the coolant level inside the vessel, T_s the molten salt temperature and T_a the air temperature: the temperature gradient, moving with the coolant level, originates the stresses (from Reference [8]).

the cylinder walls. Similarly, the stresses applied to the structure of a reactor vessel are mainly linked to the movement of such axial thermal gradient, since at the free surface the primary loads are low or negligible. By validated computational methods, the related uncertainties and risks of progressive deformation can be reduced, while ensuring that plant designs still remain conservative [9].

Within this frame, the Euratom Horizon 2020 Project Generation IV Materials Maturity (GEMMA) has been ongoing since 2017 [10], with the general objective to qualify and codify the selected structural materials for the construction of Gen IV reactors as envisaged by the European Sustainable Nuclear Industrial Initiative (ESNII) [11]. One of the GEMMA work packages is devoted to micro-structural characterization of welded components, determining welding residual stresses, establishing test procedures and deriving reference material data on mechanical properties in air. The aim is to provide recommendations for adapting or developing assessment procedures and design rules in the RCC-MRx design code [7] for nuclear welded components.

The experimental results presented in this paper have been obtained in the frame of this GEMMA Project work package, utilizing the neutron diffraction technique to obtain the distribution of residual stresses in a 316L(N) weld, manufactured and specifically instrumented to facilitate modeling of residual stresses as well as of post-weld heat treatment effects. In fact, as shown also by the results here below, neutron diffraction is unique in probing micro-structural and crystallographic changes in massive steel samples, down to depths of several mm below the surface. Furthermore it is a non-destructive technique; therefore the same sample can be investigated, after the neutron measurements, by other destructive or semi-destructive techniques, or be submitted to thermo-mechanical treatments to investigate unambiguously how its initial metallurgical state and residual stress distribution are modified. Namely, the same model weld described in the next section will be submitted to a mitigation post-weld dimensional heat treatment, to subsequently investigate its effectiveness in reducing the stress concentrations, particularly at the weld and the HAZ. Therefore, the results presented here below constitute a first achievement in a step-by-step approach aimed to experimentally validate mitigation procedures useful to improve the safety of nuclear welds. These results will serve as a benchmark for related numerical welding models.

Material characterization

The investigated sample had been prepared by the CEA laboratories at Saclay, France [12-14]. The weld was obtained by a Tungsten Inert Gas (TIG) Narrow Gap (NG) fully mechanized welding process, optimized for weld thicknesses of up to 60 mm of 316L/316L(N) grade stainless steel. The chemical composition of the base material, austenitic stainless steel 316L(N), and of the filler material (solid wire 18Cr-12Ni-2Mo) are reported in Table 1. The wire grade of the filler is not included in the RCC-MRx Code; the measurements therefore also contribute to verifying suitability of this innovative austeno-ferritic filler for austenitic stainless steels. The weld was obtained by a Tungsten Inert Gas (TIG) Narrow Gap (NG) fully mechanized welding process, optimized for weld thicknesses of up to 60 mm of 316L/316L(N) grade stainless steel. A multipass procedure was adopted, with 11 runs to fill the narrow gap completely. Automatic mode, pulsed current, a lanthanum electrode (diameter of 3.2 mm, WLa20 Lanthanum 2 %), argon as shielding gas and maximum interpass temperature of 150° were selected as general welding parameters. Current intensity was 140–310 A, voltage 9–10 V, travelling speed 8–12 cm/min [14]. Optical micrographic observation showed that the average grain size in the base metal is approximately 40 μm; the HAZ is not uniform in width, with heterogeneous distribution of coarsened austenitic grains and delta ferrite, and dendritic structures appear inside the weld [14]. The Vickers micro-hardness, measured across the weld, is nearly constant around 220 MHV within ± 10% approximately [14].

Fig. 2 shows a section of this weld, namely the coupon utilized for obtaining the un-strained reference samples, and the scheme of the positions selected for stress mapping of the weld itself. The sample dimensions are 305 mm long, 295 mm wide and 24 mm thick. The coupon displays an angular distortion of approximately 4° as a result of the manufacturing process. Two strain-free reference samples, one for base metal and one for the weld, were prepared in the shape of rods obtained from one of the slices cut from the original weld, as shown in Fig. 2. This sample utilized for the neutron diffraction measurements had been obtained from a weld originally 325 mm long. Several slices 5 mm long have been cut from the ends of this original weld, in order not to modify the stress distribution at mid-length, for different destructive or semi-destructive analyses: scanning electron microscopy (SEM), X-ray diffraction, Electron Backscatter Diffraction (EBSD) and small-punch tests [12].

Experimental technique

Reference is made to [15] for a general presentation on the use of neutron diffraction for stress determination and to [16-22] for some applications to nuclear welds. The measurement of strains and stresses by neutron or X-ray diffraction is based on the Bragg law.

$$2d_{hkl}\sin\theta = n\lambda \tag{1}$$

relating the spacing, d_{hkl}, between crystallographic lattice planes characterized by Miller indices *hkl* to the wavelength, λ, of the neutrons or X-rays and the angle 2θ where the corresponding reflection is observed. The main advantage of utilizing neutron beams with respect to X-rays is their deeper penetration into the materials, up to several mm in steels, compared to a penetration depth in the range 1 to 100 μm for X-rays. When defining the strain ε as:

$$\varepsilon = \frac{(d - d_0)}{d_0} \tag{2}$$

Table 1
Chemical composition (wt%, Fe bal) for base and filler material.

Base material AISI 316 L(N)											
C	Si	Mn	P	S	Cr	Mo	Ni	N	Cu	Co	B
0.026	0.31	1.74	0.025	0.001	17.27	2.54	12.13	0.069	0.29	0.09	0.0004

Filler material solid wire 18Cr-12Ni-2Mo															
C	Si	Mn	P	S	Cr	Mo	Ni	N	Cu	Co	Al	Nb	Ti	B	Ta
0.044	0.513	1.318	0.013	0.0033	18.236	1.953	11.526	0.064	0.097	0.001	0.006	0.001	0.001	0.0004	0.005

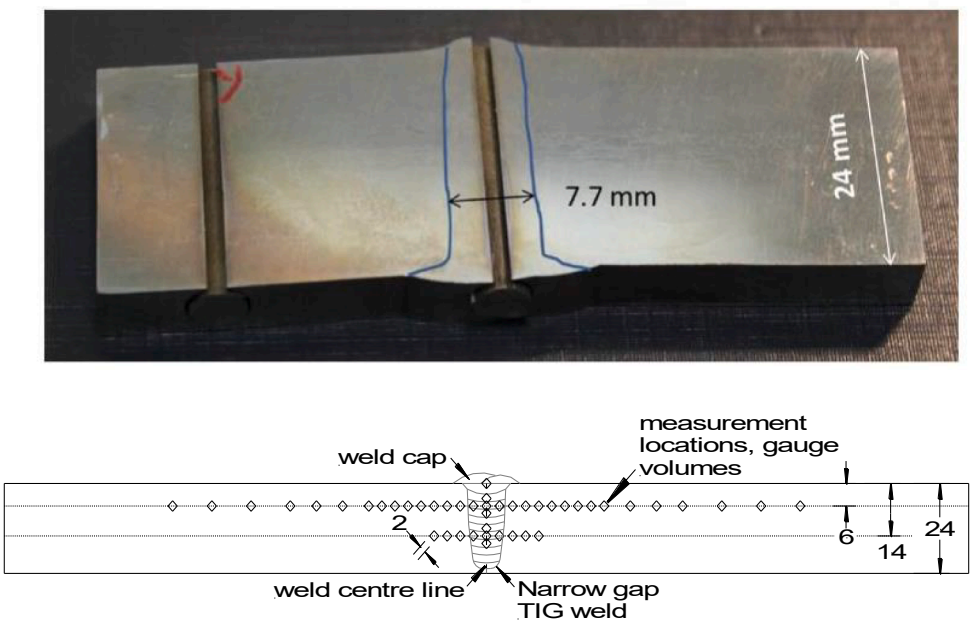

Fig. 2. Top: cross-sectional picture of 5 mm thick slice obtained from the original 316L(N) TIG narrow gap weld, including the un-strained, rod-shaped reference samples obtained in the base metal and inside the weld. Bottom: locations selected for the neutron diffraction measurements in the 295 mm wide weld.

where d and d_0 are the strained and un-strained lattice parameters respectively, ε can be determined by the shift in the position of the Bragg peaks. The broadening of these peaks is determined through the changes of their full width at half maximum (FWHM), which is related to crystallographic grain size, defect density or local variations of strain. Following Equation (2) there is a need for a 'strain-free' sample, with lattice spacing d_0, in order to calculate absolute residual strains. In general, if *X, Y, Z* are defined as three mutually orthogonal directions at a measurement location inside a sample, then the normal residual stress components at that location are given by:

$$\sigma_X = \frac{E_{hkl}}{(1+\upsilon_{hkl})(1-2\upsilon_{hkl})}[(1-\upsilon_{hkl})\varepsilon_X + \upsilon_{hkl}(\varepsilon_Y+\varepsilon_Z)],$$

$$\sigma_Y = \frac{E_{hkl}}{(1+\upsilon_{hkl})(1-2\upsilon_{hkl})}[(1-\upsilon_{hkl})\varepsilon_Y + \upsilon_{hkl}(\varepsilon_X+\varepsilon_Z)], \quad (3)$$

$$\sigma_Z = \frac{E_{hkl}}{(1+\upsilon_{hkl})(1-2\upsilon_{hkl})}[(1-\upsilon_{hkl})\varepsilon_Z + \upsilon_{hkl}(\varepsilon_X+\varepsilon_Y)]$$

where E is the Young's modulus of the investigated material and ν the Poisson's ratio; both E and ν are diffraction elastic constants depending on the *hkl* reflection, i.e E_{hkl} and ν_{hkl}. When *X*, *Y*, and *Z* are defined as the welding longitudinal, welding transverse and plate normal directions, it is reasonable to assume that these are also the principal stress directions for this sample in the region of measurement, as it is also shown in References [23,24].

The neutron diffraction measurements were carried out at room temperature utilizing the STRESS-SPEC diffractometer [25], at the FRM-II reactor in Garching, Germany. A neutron wavelength of 1.48 Å, produced by a Si(0 0 4) monochromator, was utilized to investigate the ⟨3 1 1⟩ crystallographic reflection of the 316L(N) austenitic steel. Fig. 3 shows the orientation of the principal stress directions (longitudinal, transverse and normal) and the experimental layout to measure each of them. Namely, the transverse strains were measured by rotating the sample by 90° around the weld direction, with respect to the orientation shown in Fig. 3(a), which represents the measurements in the plate normal direction. The selected neutron gauge volumes were the following: $2 \times 2 \times 10$ mm^3 in the transverse direction, $3 \times 3 \times 2$ mm^3 in the longitudinal direction, and $2 \times 2 \times 10$ mm^3 in the plate normal direction, with the long 10 mm dimension always aligned in the direction parallel to the weld. Accurate positioning of the sampling volume inside the specimen was ensured probing the variation of the diffracted intensity when moving a sample surface through the gauge volume. Analysis of data obtained by such "entry scans" allows determining the position of the sample surface with respect to the gauge volume with an achievable accuracy lower than 0.1 mm, as it is also shown in Reference [26]. Doing at least two entry scans on either side of the sample also ensured that the angular distortion of the coupon was correctly accounted for in the positioning of the gauge volumes. The neutron diffraction measurements were carried out along a line perpendicular to the weld direction, at mid-length in the sample, at two different depths below the cap side of the plate: approximately 6 mm and 14 mm. Additional measurements were carried out in the centre of the weld, at 7 different depths below the cap side, down to 16 mm. During the different scans, the sample was oscillated to mitigate grain size spurious effects.

Measurements of the unstrained lattice parameter (d_0), in the three

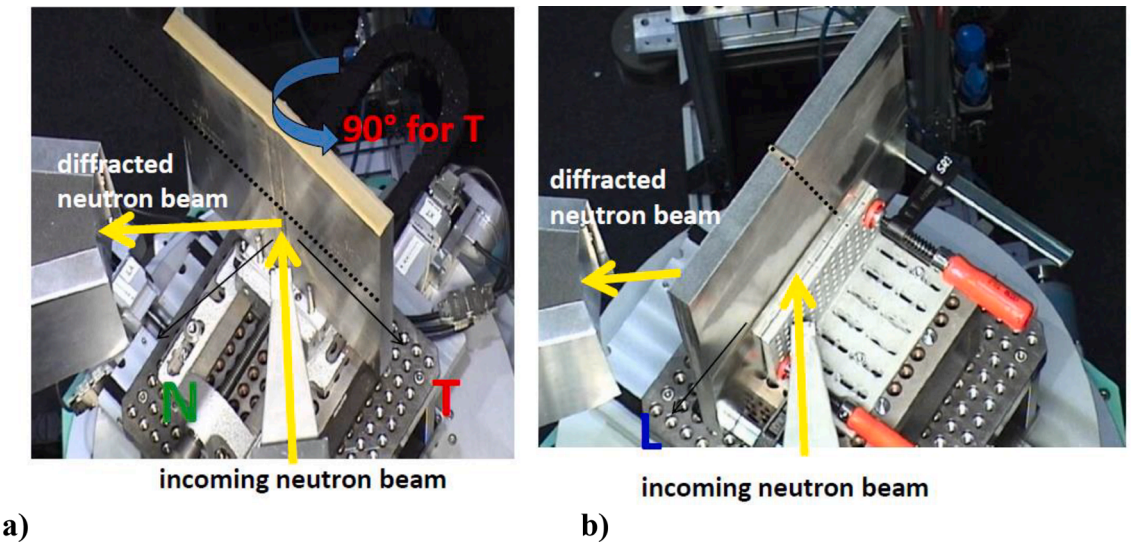

Fig. 3. Experimental layout for the measurement of the full stress tensor in the 316L(N) TIG narrow gap weld: a) layout for plate normal (N) and welding transverse (T) direction strains, b) layout for welding longitudinal (L) direction strains. The measurements were carried out scanning the sample along the dotted line, at its mid-length, perpendicularly to the weld direction.

principal directions, for strain determination in accordance with Equation (2) were done using two 5 mm diameter rods, cut by wire erosion from the base metal and the weld at the weld centre line, respectively, as shown in Fig. 2. The 5 mm diameter is too small for the rods to still contain any macroscopic residual stresses; therefore, these specimens were considered suitable for the reference measurements. Measurements at various locations and in several directions in the base metal rod showed low variations in the lattice spacing only. Therefore, an average reference value was determined, and this single value was used for all calculations of strain for locations in the base metal. In austenitic stainless steels, often the reference value in the weld deviates from that for the base metal and the reference value varies with location and with measurement direction. This is due to chemistry variations, but also to the differences in thermo-mechanical history between different locations in the weld. In order to account for these effects, an individual reference value was measured on the rod extracted from the weld for every measurement location at weld centre line in all three measurement directions. These individual values were then used for the strain and stress calculations inside the weld.

The SteCa 2 software [27] has been utilized to analyze the neutron diffraction data and to subsequently obtain the strains and the stresses. The diffraction elastic constant $E_{311} = 183.6$ MPa was used with a corresponding Poisson's ratio $\nu_{311} = 0.306$ [28] for the conversion of strain to stress in accordance with Equation (3). The experimental errors on the measured strains and stresses, due to neutron counting statistics, were determined as described in References [25,26]. Under the selected experimental conditions, an uncertainty of $\pm 0.004°$ is associated to the determination the diffraction peak position, with corresponding uncertainties of $\pm$ 42 μm/m for the measured strains and of $\pm$ 12 MPa for the measured stresses.

Results

Figs. 4 and 5 show the three strain and stress components measured as a function of the distance from the weld centre at 6 mm depth and at 14 mm depth, respectively. At each depth, similar trends as a function of the distance from the weld centre are found for strains and stresses; the stresses are mostly concentrated within a region approximately $\pm$ 5 mm distant from the weld center. At 6 mm depth, a marked and narrow tensile stress gradient is detected around the centre of the weld for the longitudinal and transverse direction, the first one raising up to 400 MPa approximately. At 14 mm depth, in the centre of the weld, much lower tensile stresses are found in the longitudinal direction, with smoother gradient, while in the transverse direction compressive stresses are found as low as −200 MPa approximately. These changes are highlighted in Fig. 6, comparing how each stress component varies with increasing the depth below the weld cap. Comparing all these results with those obtainable by conventional methods, like micro-hardness [14], much more detailed information is obtained on the stress state of the sample in its most critical region: not only the longitudinal and transverse stresses vary significantly within the HAZ and weld center, but additionally their gradients appear dependent on the depth inside the sample, at least for the two investigated depths. Namely, due to their limited penetration depth and sampling volume, compared to neutron diffraction, the micro-hardness measurements respond in a different way to the complex metallurgical transformations occurring in the weld centre and in the HAZ. Furthermore, in this particular case, only limited hardness variation was found between the base material and the weld material, whereas significant residual stress changes are observed. The same has been found for a different weld, a multipass SMAW weld, manufactured from the same base material for the same project [29]. It is also noted that according to some literature on AISI 316L welds (see for instance Reference [30]), hardness measurements not always show the same trends as other methods especially in the weld itself, often due to grain size issues.

The three strain and correspondingly calculated stress components measured inside the weld centre as a function of the depth below the weld cap are shown in Fig. 7. Also these in-depth measurements confirm that the main integrity concern for the investigated sample may arise from the tensile longitudinal stresses. Furthermore, these data suggest that inside the weld the three stress components vary in a complex way with the depth, probably due to the metallurgical changes detected by metallography [14]. However, it would be difficult to obtain more quantitative and predictive information on such effect without more accurate observation by local techniques and possibly by stress measurements extended more in the depth.

The FWHM's measured in each series of scanning through the sample are shown in Fig. 8 for each strain component. These FWHM's have been obtained as the peak width output of the fit of the corresponding reflection, without correction for instrumental broadening, expected to be a constant. Therefore, they are presented solely for the purpose of adding qualitative information to the stress measurements. Namely,

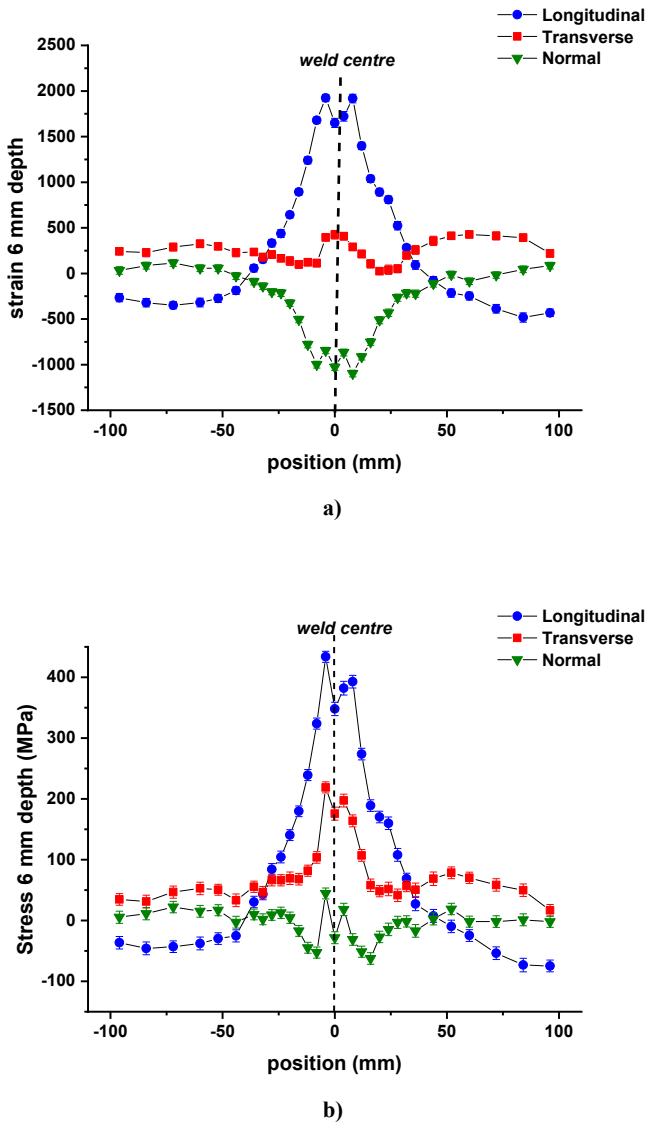

Fig. 4. Strains $\times 10^6$ (a) and stresses (b) as a function of the distance from the weld centre, at 6 mm depth below the surface of the weld for the three measurement directions: longitudinal (circles, blue), transverse (squares, red), normal (triangles, green).

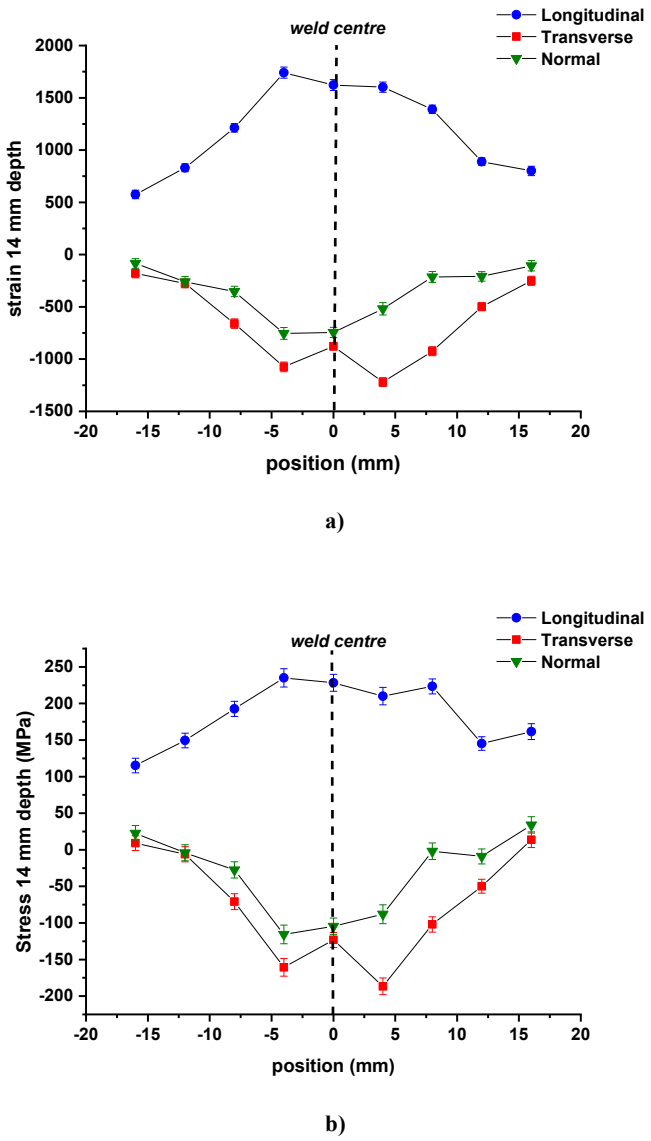

Fig. 5. Strains $\times 10^6$ (a) and stresses (b) as a function of the distance from the weld centre, at 14 mm depth below the surface of the weld for the three measurement directions: longitudinal (circles, blue), transverse (squares, red), normal (triangles, green).

Fig. 8 shows that significant metallurgical changes, to be related to plastic deformation, occur in a narrow area about ± 20 mm on either side of the weld centre line. That area is narrower than the tensile region shown in Fig. 4 (±36 mm), but clearly wider than the fusion zone itself (7.7 mm total) shown in Fig. 2. No significant variations were observed inside the weld, as shown in Fig. 8 (c), with the exception of the capping pass location where the FWHM is approximately at the level of that in the base material for two measurement directions. The latter could be explained by the fact that the capping passes of the weld have experienced fewer thermo-mechanical load cycles than the passes deposited earlier and have therefore gone through less plastic and cyclic deformation.

Comparing, even just qualitatively, such results with those obtained by neutron diffraction on different AISI 316 welds [16-22,31] is not straightforward due to the different welding methods and samples geometries. However, the development of longitudinal stresses higher than 300 MPa inside the weld and its dependence with the depth below the weld cap seems to be a general feature, particularly considering the results obtained on the hybrid weld described in Reference [22].

Discussion and conclusions

Neutron diffraction has been successfully utilized for obtaining in a non-destructive way an accurate mapping of the stress distributions in a model nuclear weld, down to a depth of 16 mm below its surface. No other experimental technique allows obtaining such information, essential to assess and possibly validate numerical stress evaluations, where the influences of the complex thermo-mechanical cycles of the welding process, the effects of the restraint during welding, and the finite size of the specimen are difficult to take into account. It is worth noting that with access to an intense neutron source and to a high-resolution instrument, like the one utilized here STRESS-SPEC at FRM-II, these results can be obtained in a neutron beam-time of 24 h. The obtained stress distributions are affected by experimental uncertainties of a few % on the stress values themselves. Such level of accuracy is very important in view of comparing these experimental stress results with those of numerical simulations, in progress for this same model weld [32]. Deeper metallurgical investigation of the weld centre, both by diffraction line profile analysis and by destructive metallography, would

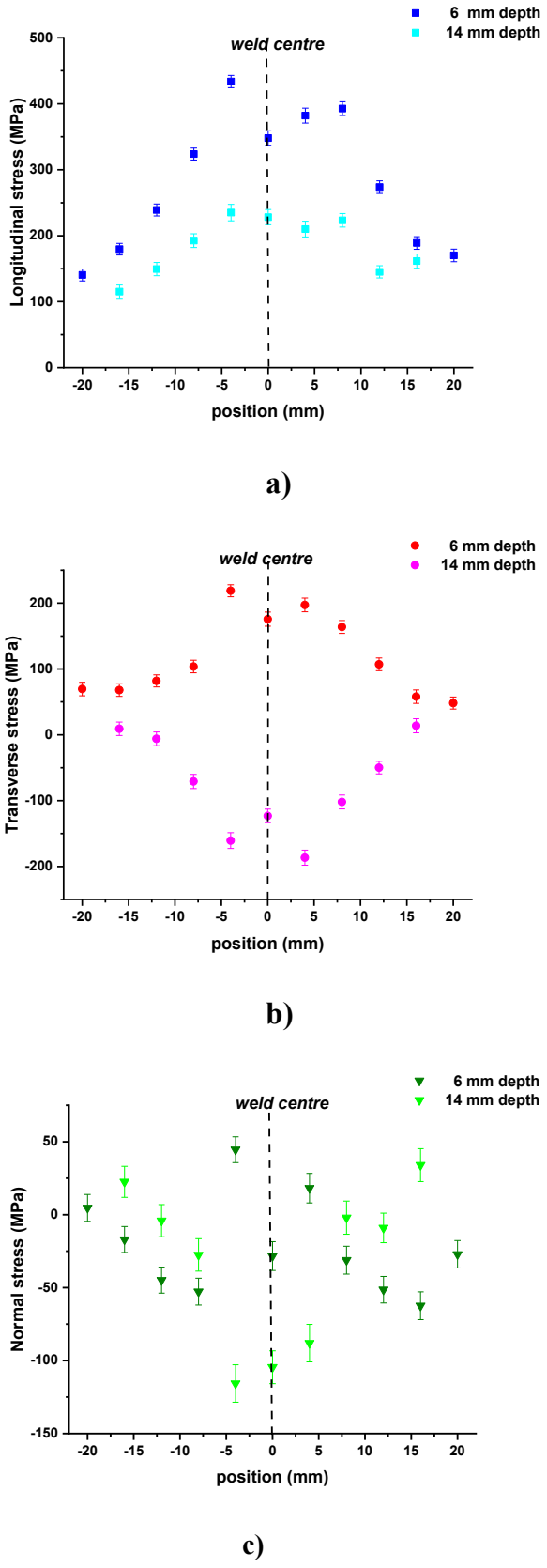

Fig. 6. Comparison of longitudinal (a), transverse (b) and normal (c) stresses at 6 mm and 14 mm depth, inside the weld and the HAZ.

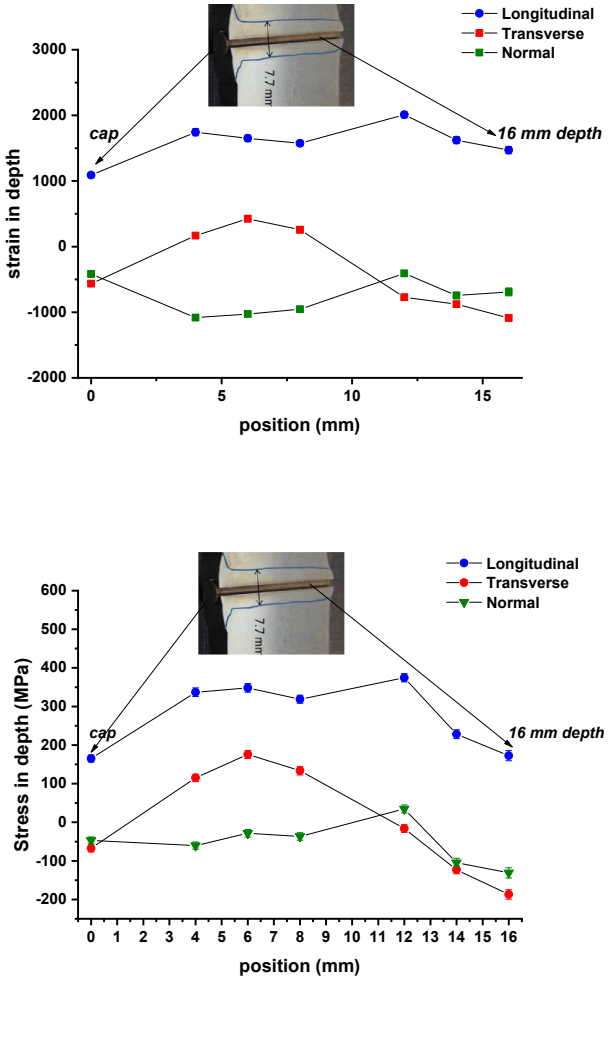

Fig. 7. Strains $\times 10^6$ (a) and stresses (b) as a function of the distance from the weld cap in the centre of the weld, for the three measurement directions: longitudinal (circles, blue), transverse (squares, red), normal (triangles, green).

provide an important contribution for modeling purposes.

The experimentally obtained stress distributions show that the weld appears as a narrow-gap one also from the micro-structural viewpoint, with stresses concentrated in a well-defined and restricted region around the weld centre. This confirms from a micro-structural viewpoint the accuracy of the metallurgical protocol adopted to prepare the investigated weld [13,14]. However, the high values of the longitudinal stress component should be carefully taken into account as far as nuclear safety is concerned and the implementation of mitigating techniques is needed before utilizing such welds in the plant. It should also be noted that the thickness of welds to be effectively utilized for reactor vessel walls will be considerably higher (60 mm) than that of the sample investigated (24 mm). Therefore, the metallurgical results obtained by the present work should be extrapolated in a conservative way and confirmed by additional measurements of real-scale welds. Furthermore, components of interest are typically not flat. Pipe welds have a completely different restraint situation, normally leading to different stress distributions. It must also be noted that, as indicated by the measurements, residual stresses are already at the yield stress level reached after hardening in the weld. There is therefore limited room for scaling the maximum stress with thickness. Based on joint scientific work carried out within the GEMMA Project, a heat treatment with a dwelling time of 24 h at 700 °C, with limited heating and cooling rates, appears as the best suited one for mitigating the post-weld stress

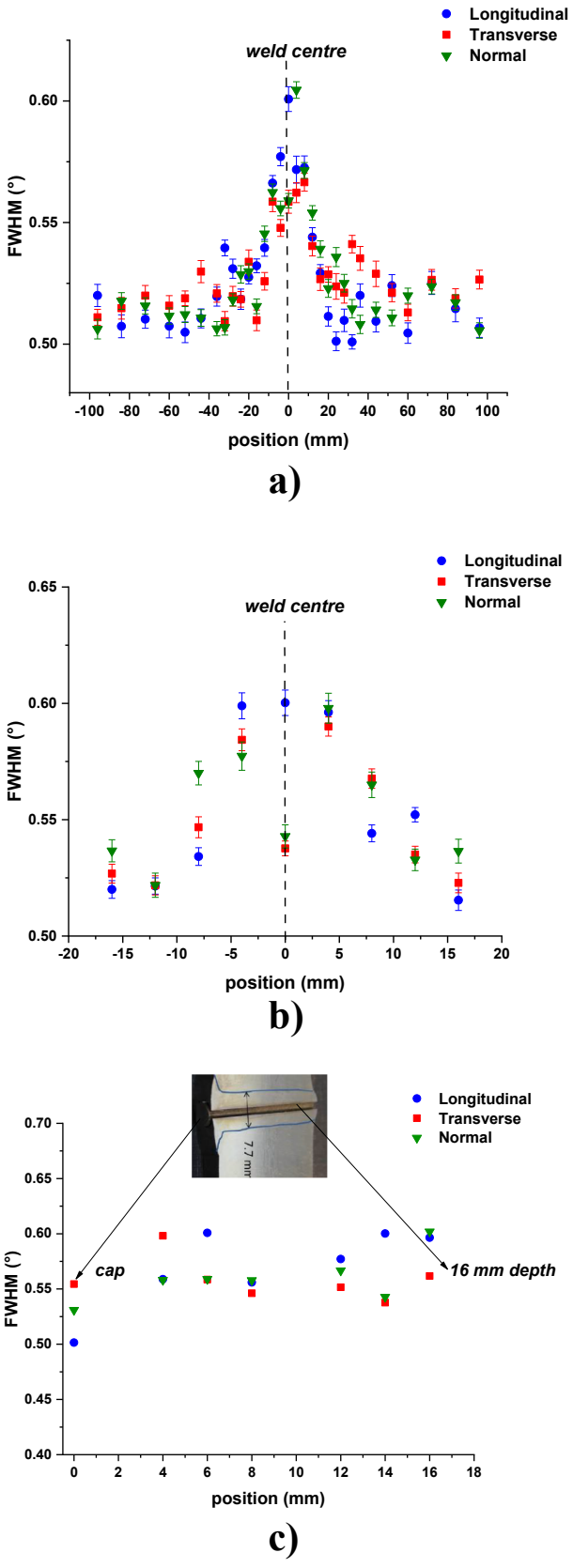

Fig. 8. FWHM (°) measured as function of distance from the weld centre at 6 mm depth (a) and at 14 mm depth (b), and measured as a function of distance from the weld cap in the centre of the weld (c) for the three measurement directions: longitudinal (circles, blue), transverse (squares, red), normal (triangles, green).

distributions detected in this weld. The relatively high temperature and long dwelling time were chosen to ensure that a tangible relaxation of residual stressed would be attained by the treatment. These specifications were selected to fulfil a scientific interest in the process. The relation of the heat treatment process to the RCC-MRx code is limited. Experimental results, including new stress measurements, on the effect of such treatement in this same 316L(N) TIG-NG weld will be the object of future scientific publications.

CRediT authorship contribution statement

P. Agostini: Resources, Conceptualization. **R. Coppola:** Conceptualization, Investigation. **M. Hofmann:** Investigation, Software, Formal analysis, Data curation. **C. Ohms:** Investigation. **K. Tucek:** Conceptualization.

Declaration of Competing Interest

The authors declare that they have no known competing financial interests or personal relationships that could have appeared to influence the work reported in this paper.

Acknowledgments

The research leading to these results has been carried out in the frame of the EERA Joint Programme on Nuclear Materials and is partly funded by the European Commission HORIZON 2020 Framework Programme under grant agreement No. 755269.

References

[1] Technology Roadmap for Generation IV Nuclear Energy Systems, Technical Report GIF-002-00, 2002.
[2] Technology Roadmap Update for Generation IV Nuclear Energy Systems, Technical report GIF, 2014.
[3] GIF R&D Outlook for Generation IV Nuclear Energy Systems: 2018 Update, Technical report GIF, 2018.
[4] P. Yvon, M. Le Flem, C. Cabet, J.L. Seran, Structural materials for next generation nuclear systems: Challenges and the path forward, Nuclear Engineering and Design 294 (2015) 161–169, https://doi.org/10.1016/j.nucengdes.2015.09.015.
[5] K. Tucek, H. Tsige-Tamirat, L. Ammirabile, A. Làzaro, A. Grah, J. Carlsson, Ch. Döderlein, M. Oettingen, M.A. Fütterer, E. D'Agata, M. Laurie, K. Turba, C. Ohms, K.-F. Nilsson, P. Hähner, Generation IV Reactor Safety and Materials Research by the Institute for Energy and Transport at the European Commission's Joint Research Center, Nuclear Engineering and Design 265 (2013) 1181–1193, https://doi.org/10.1016/j.nucengdes.2013.06.018.
[6] G.A. Young, J.D. Tucker, M.J. Hackett, Welding Challenges in Generation IV Nuclear Systems, Transactions of the American Nuclear Society 102 (1) (2010) 704–706. https://www.researchgate.net/publication/262731959.
[7] AFCEN (2013).
[8] G. Aiello, P. Matheron, K. Zhang, J. Aktaa, M. E.Angiolini, G. M. Giannuzzi, D. Mele, L.Pilloni, L. Sipione, *Recommendation for ratcheting rules for P91 components*, MATTER Material Testing and Rules Grant, Deliverable D4.4 report (2015).
[9] IAEA, Safety of Nuclear Power Plants: Design, Specific Safety Requirements, SSR-2/1, Rev. 1, 2016.
[10] http://www.eera-jpnm.eu/gemma/.
[11] https://snetp.eu/esnii/.
[12] https://cordis.europa.eu/project/id/755269/results.
[13] O. Doyen, CEA Report DEN/DANS/DM2S/SEMT/LTA/NT/ 2018-62467/A, March 2018.
[14] L. Forest, CEA Technical Report DEN/DANS/DM2S/SEMT/LTA/NT/2018-64038/B. April 2019.
[15] M.T. Hutchings, P.J. Withers, T.M. Holden, T. Lorentzen, Introduction to the Characterization of Residual Stress by Neutron Diffraction, Taylor & Francis (2005), https://doi.org/10.1201/9780203402818.
[16] G.D. Bokuchava, P. Petrov, I.V. Papushkin, Application of neutron stress diffractometry for studies of residual stresses and microstrains in reactor pressure vessel surveillance specimens reconstituted by beam welding methods, Journal Surface Investigation 10 (6) (2016) 1143–1153, https://doi.org/10.1134/S1027451016050463.
[17] G.D. Bokuchava, P. Petrov, Study of Residual Stresses and Microstructural Changes in Charpy Test Specimens Reconstituted by Various Welding Techniques, Metals 10 (2020) 632, https://doi.org/10.3390/met10050632.
[18] C. Ohms, R.V. Martins, O. Uca, A.G. Youtsos, P.J. Bouchard, M. Smith, M. Keavey, S.K. Bate, P. Gilles, R.C. Wimpory, L. Edwards, *The European Network on Neutron Techniques Standardization for Structural Integrity – NeT*, in: Proceedings of ASME

PVP 2008, Chicago, USA, July 27-31, 2008, ASME, CD Publication, 2008, Order No. I795CD, ISBN 0-7918-3828-5.
[19] M.C. Smith, A.C. Smith, R.C. Wimpory, C. Ohms, *A review of the NeT Task Group 1 residual stress measurement and analysis round robin on a single weld bead-on-plate specimen*, International Journal of Pressure Vessels and Piping, Vol. 120-121, Aug-Sep, 2014, pp. 93-140, DOI: 10.1016/j.ijpvp.2014.05.002.
[20] S. Pratihar, M. Turski, L. Edwards, P.J. Bouchard, Neutron diffraction residual stress measurements in a 316L stainless steel bead-on-plate weld specimen, International Journal of Pressure Vessels and Piping 86 (2009) 13–19, https://doi.org/10.1016/j-ijpvp.2008.11.010.
[21] J. Katsuyama, M. Nakamura, T. Tobita, K. Onizawa, Effects of shape of weld and welding conditions on residual stress at welded joints of stainless steel piping, in: In: Preprints of the National Meeting of JWS. Japan Welding Society, 2009, p. 37.
[22] P. Agostini, G. Barbieri, R. Coppola, M. Moncada, C. Ohms, R.C. Wimpory, Stress Distributions in P91 Martensitic Steel and in AISI 316 LN Steel Welds for Gen IV Nuclear Applications, Journal of Surface Investigation 14 (2020) S25–S30, https://doi.org/10.1134/S1027451020070022.
[23] S. Spooner M.E. Fitzpatrick A. Lodini . Taylor&Francis, Analysis of Residual Stress by Diffraction using Neutron and Synchrotron Radiation 2003 296. https://doi.org/10.1201/9780203608999.
[24] J. Rebelo Kornmeier, M. Hofman, W.M. Gan, V. Robin, F. Valiorgue, H. Pascal, J. Gibmeier, J. Saroun, Effects of finish turning on an austenitic weld investigated using diffraction methods, The International Journal of Advanced Manufacturing Technology 108 (2020) 635–645, https://doi.org/10.1007/s00170-020-05386-8.
[25] Journal of large-scale research facilities 1 2015 A6 https://doi.org/10.17815/jlsrf-1-25.
[26] R.S. Ramadhan, S. Cabeza, T. Pirling, S. Kabra, M. Hofmann, J. Rebelo Kornmeier, A.M. Venter, D. Marais, Quantitative analysis and benchmarking of positional accuracies of neutron strain scanners, Nuclear Instuments and Methods in Physics Research A 999 (2021), 165230, https://doi.org/10.1016/j.nima.2021.165230.
[27] C. Randau, U. Garber, H.-G. Brokmeier, StressTextureCalculator: a software tool to extract texture, strain and microstructure information from area-detector measurements, Journal of Applied Crystallography 44 (2011) 641–646, https://doi.org/10.1107/S0021889811012064.
[28] Wen Chen Zhang, David L. McDowell, Y. Morris Wang, Ting Zhu, *Lattice strains and diffraction elastic constants of cubic polycrystals*, Journal of the Mechanics and Physics of Solids 138 (2020), https://doi.org/10.1016/j.jmps.2020.103899.
[29] C. Ohms *et al.*, to be published.
[30] O. Muransky, M. Tran, C.J. Hamelin, S.L. Shrestha, D. Bhattacharyya, Assessment of welding-induced plasticity via electron backscatter diffraction, International Journal of Presssure Vessels and Piping 164 (2018) 32–38, https://doi.org/10.1016/j.ijpvp.2017.04.001.
[31] R.C. Wimpory, C. Ohms, M. Hofmann, R. Schneider, A.G. Youtsos, Statistical analysis of residual stress determinations using neutron diffraction, International Journal of Pressure Vessels and Piping 86 (2009) 48–62, https://doi.org/10.1016/j.ijpvp.2008.11.003.
[32] W. Sun *et al.*, to be published.